Nondestructive evaluation of ferromagnetic material thickness using Pulsed Eddy Current sensor detector coil voltage decay rate

Nalika Ulapane[a], Alen Alempijevic[a,*], Jaime Valls Miro[a], Teresa Vidal Calleja[a]

[a] *Centre for Autonomous Systems, University of Technology Sydney, 15 Broadway, Ultimo, NSW 2007, Australia*

Abstract

A novel ferromagnetic material thickness quantification method based on the decay rate of a Pulsed Eddy Current sensor detector coil voltage is proposed. An analytical expression for the decay rate is derived and the relationship with respect to material thickness, in particular that of large diameter pipes, is validated through finite element analysis and experiments. The relationship is verified to hold for a range of ferromagnetic materials and subsequently used for wall thickness quantification of in situ pipes. Estimated pipe wall thickness is evaluated after destructive testing and graphitisation removal. Lift-off insensitivity and potential for thickness estimation through nonconducting coatings is discussed.

Keywords: detector coil, ferromagnetic, finite element analysis, Pulsed Eddy Current, pipe, sensor

1. Introduction

The Pulsed Eddy Current (PEC) technology is considered as a more versatile member of the family of Eddy Current (EC) Nondestructive Evaluation (NDE) techniques [1]. Since EC inspection techniques are severely affected by the skin

*Corresponding author

Email addresses: Nalika.Ulapane@uts.edu.au (Nalika Ulapane), Alen.Alempijevic@uts.edu.au (Alen Alempijevic), Jaime.VallsMiro@uts.edu.au (Jaime Valls Miro), Teresa.VidalCalleja@uts.edu.au (Teresa Vidal Calleja)

effect, they are commonly used on nonmagnetic or magnetic materials with low relative permeability [2]. The broad frequency spectrum incorporated with PEC signals has enabled the technology to overcome to a reasonable extent the skin effect limitation. Previous research has demonstrated the applicability of PEC technology on ferromagnetic materials, with a particular focus on flaw detection [3, 4, 5]. Therefore, advancing PEC technologies in relation to ferromagnetic material NDE has become a significant present day research interest as many existing pipeline systems throughout the world are aging and reaching their design lifetimes [6]. This paves way for PEC technology to be highly effective on condition assessment of in situ ferromagnetic critical pipes [3, 7].

Traditional PEC signal features used for evaluating test piece properties and defect quantification can be classified as: time domain signal features [8, 9], frequency spectrum features [10, 11], principal components [12, 13] and integral features [14, 15]. Some specific features among those which have been found to be effective on ferromagnetic materials for defect detection are presented in [4, 16] while features used for thickness estimation are discussed in [8, 17]. In [16], a remote field eddy current sensor has been energized by a PEC excitation to detect axisymmetric surface slot defects on ferromagnetic tubes by examining the variations of the induced detector coil voltage features. Using magnetization to improve the sensitivity of the time domain reference subtracted PEC difference signal features was proposed in [4] to detect and quantify subsurface defects in ferromagnetic steels. Although the features used in [4] and [16] are effective on defects, their effectiveness on ferromagnetic material thickness quantification has not been examined. With respect to thickness estimation, [8] proposes using the 'time-to-peak' feature of the PEC difference signal for assessment of wall thinning of ferromagnetic pipes. However, authors have admitted that the feature is effectively usable for a limited range of relative wall thinning and has been examined only on steel. Several analytical models that can be used for thickness quantification have also been proposed [17, 18, 19]. References [18] and [19] follow similar approaches in modeling PEC difference signals and hall effect sensor readings respectively, when used on non-ferromagnetic materials.

In the context of ferromagnetic materials however, sensitivity of those sensing techniques to thickness becomes overshadowed by the sensitivity to material permeability [1]. Consequently, the presented techniques are not generally used for thickness estimation of ferromagnetic materials. In recent work [17] and [20] analytical models for PEC sensors having detector coils as receivers are presented. As opposed to the sensing techniques in [18] and [19], the induced detector coil voltage has been observed to exhibit better sensitivity to ferromagnetic material thickness when subjected to some signal conditioning steps and scale transformations [5, 17, 20]. Based on that knowledge and explicit focus on ferromagnetic materials, this paper proposes to use a detector coil based PEC sensor.

The main objective of this paper is to propose a method for estimating thickness of in situ ferromagnetic materials, in particular that of critical water pipes. A method of using the decay rate of the time domain induced detector coil voltage of a PEC sensor to quantify ferromagnetic material thickness based on an analytical relationship derived between the decay rate and material thickness is presented. We start our derivation using the circuit theory based generic PEC signal model proposed in [17]. In contrast to [17] and [20] where an analytical model is fitted to the raw signal and the variation of model parameters is used for thickness discrimination, we propose the signal decay rate as an alternative option with a convenient practical advantage of being directly extractable from raw PEC signals. As with any other NDE technique, practical application of the proposed method requires accurate calibration and this gradient feature formulation allows convenient calibration by means of estimating material electrical and magnetic properties or performing ultrasound measurements on coupons having known thickness. Validation of the applicability of this method on large diameter cylindrical structures is specifically investigated, the analysis is done using Finite Element Analysis whilst incorporating material property and sensor characteristics. Tests performed to verify the usability of the decay rate for in situ NDE of ferromagnetic pipes located in commercial water utility environments yielded a percentage accuracy of over 90% when quantitatively compared

to the actual ferromagnetic material thickness after destructive testing. We also report experimentally observed lift-off insensitivity associated with the decay rate feature to discuss potential for thickness assessment of coated metallic structures.

The breakdown of this paper is as follows: Section 2 presents the analytical derivation of the relationship between the decay rate and thickness. Finite element analysis validation of the approach for cylindrical structures is presented in Section 4 and experimental validation of the generalization of this method for a range of ferromagnetic materials is explained in Section 5. The application of the method on in-situ ferromagnetic pipes of a water utility are presented in Section 6 with a discussion on their implications. The paper concludes in Section 7 with remarks on the proposed method of PEC detector coil voltage decay rate based ferromagnetic material thickness quantification.

2. Analytical deviation of decay rate feature

A detector coil based PEC sensor placed above a conducting test piece, when not affected by external sources of noise, can be modeled in circuit theory as a setup composed of infinitely many mutually coupled coils [17]. Such an analysis yields an analytical model Eq. 1 which represents the decaying part of a PEC induced detector coil voltage

$$V(t) = \sum_{i=1}^{\infty} b_i \exp\left(-c_i t\right). \tag{1}$$

Terms b_i and c_i are constants which contain the properties of the sensor setup and the test piece and the condition $c_i > 0$ holds for all i [17]. By means of linear and homogeneous representation of magnetic permeability μ and electrical conductivity σ, the diffusion time constant of eddy currents induced in a ferromagnetic plate of thickness d is defined as $\mu\sigma d^2/\pi^2$ [21]. This is the largest time constant appearing in an exponential term within the infinite summation of Eq. 1, and in return the corresponding exponential term becomes dominant in the late stage of the signal (the stage of the signal immediately before the eddy

currents decay towards zero) [21]. We therefore isolate this term and rewrite $V(t)$ as

$$V(t) = b_1 \exp\left(\frac{-\pi^2 t}{\mu\sigma d^2}\right) + \sum_{i=2}^{\infty} b_i \exp(-c_i t), \tag{2}$$

and express the natural logarithm before differentiating with respect to time to obtain the decay rate.

$$\ln[V(t)] = \ln\left[b_1 \exp\left(\frac{-\pi^2 t}{\mu\sigma d^2}\right) + \sum_{i=2}^{\infty} b_i \exp(-c_i t)\right] \tag{3}$$

The decaying part of noise free $\ln[V(t)]$ is smooth and differentiable since $V(t)$ is modeled as a sum of exponential decays as expressed in Eq. 1. The typical shape of experimental $\ln[V(t)]$ is shown in Fig. 1. Since the focus of this paper is condition assessment of ferromagnetic critical water pipes, we have chosen for our analysis gray cast iron, ductile cast iron and mild steel which are materials commonly used for manufacturing critical pipes. Fig. 1 shows signals acquired from three thicknesses of mild steel and the decay characteristic observable in the figure is generic to detector coil based PEC signals irrespective of the material being tested.

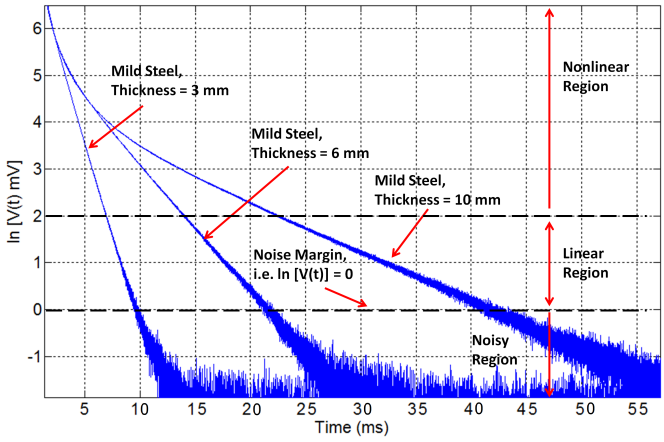

Figure 1: Typical shape of noisy $\ln[V(t)]$.

It can be seen from Fig. 1 that the initial part of a decay signal is nonlinear and reaches a linear region at a later stage, i.e. a region with constant gradient

(when noise is disregarded as in the analytical model in Eq. 1). The signal to noise ratio increases with time as the signal magnitude decreases and comes close to the inherent noise amplitude of the sensor sampling circuitry. By observing calibration signals from all three critical pipe materials, $\ln[V(t)] = 0$ was identified as a suitable noise margin for the sensor acquisition circuitry used in this work.

By fitting noise free analytical models to the decaying part of the signals above the noise margin [17], it can be observed that the constant gradient in the linear region remains unchanged as t surpasses the noise margin and tends towards very large values, i.e. $t \to \infty$ in theory. It is a fair to state that the decay rate of the linear region provides a close approximation of the decay rate $\ln[V(t)]$ at $t \to \infty$. We therefore express the decay rate of $\ln[V(t)]$ as follows:

$$\frac{\mathrm{d}\ln[V(t)]}{\mathrm{d}t} = -\frac{\dfrac{b_1\pi^2}{\mu\sigma d^2}\exp\left(\dfrac{-\pi^2 t}{\mu\sigma d^2}\right) + \displaystyle\sum_{i=2}^{\infty} b_i c_i \exp(-c_i t)}{b_1 \exp\left(\dfrac{-\pi^2 t}{\mu\sigma d^2}\right) + \displaystyle\sum_{i=2}^{\infty} b_i \exp(-c_i t)}. \tag{4}$$

By grouping exponential terms, the absolute value of the decay rate can be expressed as

$$\left|\frac{\mathrm{d}\ln[V(t)]}{\mathrm{d}t}\right| = \frac{\pi^2}{\mu\sigma d^2}\left\{\frac{1 + \displaystyle\sum_{i=2}^{\infty}\frac{b_i}{b_1}\left[\frac{c_i}{\pi^2/(\mu\sigma d^2)}\right]\exp\left[\left(\frac{\pi^2}{\mu\sigma d^2} - c_i\right)t\right]}{1 + \displaystyle\sum_{i=2}^{\infty}\frac{b_i}{b_1}\exp\left[\left(\frac{\pi^2}{\mu\sigma d^2} - c_i\right)t\right]}\right\}. \tag{5}$$

The term $\mu\sigma d^2/\pi^2$ is the largest time constant [21], therefore $c_i > \pi^2/(\mu\sigma d^2)$ holds for all i. Hence we express the main relationship used for our work, the reciprocal of the absolute value of the decay rate, as

$$\beta(t) = \left|\frac{\mathrm{d}t}{\mathrm{d}\ln[V(t)]}\right| = \frac{\mu\sigma d^2}{\pi^2}\left\{\frac{1 + \displaystyle\sum_{i=2}^{\infty}\frac{b_i}{b_1}\exp\left[-\left(c_i - \frac{\pi^2}{\mu\sigma d^2}\right)t\right]}{1 + \displaystyle\sum_{i=2}^{\infty}\frac{b_i}{b_1}\left[\frac{c_i}{\pi^2/(\mu\sigma d^2)}\right]\exp\left[-\left(c_i - \frac{\pi^2}{\mu\sigma d^2}\right)t\right]}\right\}. \tag{6}$$

By evaluating the limit of Eq. 6 as $t \to \infty$, $\beta(\infty)$ can be denoted as

$$\beta_{max} = \frac{\mu\sigma d^2}{\pi^2}. \tag{7}$$

This suggests that the decay rate is proportional to the square of the thickness and β_{max} can be used for thickness quantification conditioned on he fact PEC sensor is calibrated for a particular material (i.e. the influence of $\mu\sigma$ is quantified). In practice it is not possible to observe a $\ln[V(t)]$ at $t = \infty$, but it is indeed possible to obtain a close approximation of $\beta(\infty)$ through the linear region. We therefore extract β_{max} values from experimental signals by fitting a straight line to the linear region (i.e. $0 < \ln[V(t)] < 2$) and computing the gradient. Thus, extracted β_{max} values will satisfy the approximation Eq. 7 in order to obtain a linear model between $\ln \beta_{max}$ and $\ln d$ we opted to further model the relationship as

$$\ln \beta_{max} \approx 2 \ln d + c \tag{8}$$

where $c \approx \ln\left(\frac{\mu\sigma}{\pi^2}\right)$ is a constant for a material being tested. This approach allows to generalize the relationship by introducing a scalar offset c that encompasses the material properties μ and σ. Therefore to apply the model, c is the only parameter that requires to be estimated through calibration, in practise it can be estimated in several ways. Firstly, a material specimen can be fed through SQUID or PPMS devices to precisely measure electrical and magnetic properties. Alternatively, calibration can be performed by estimating c from signals acquired from material samples of known thicknesses. We further discuss the alternatives of estimating c in the experimental evaluation Section 5 of the paper.

3. PEC Sensor Design and Validation Against Commercial PEC Sensor

The HSK 300 commercial PEC signal capturing module [22], for which we cannot disclose specifics, is used for experiments on in situ pipes reported in

experimental evaluation Section 5. Therefore, this section demonstrates that the β_{max} feature behaves the same way irrespective of the sensor's design (rectangular or circular shape for instance) since β_{max} depends predominantly on material properties and thickness and largely independent of sensor shape and size as per the approximation in Eq. 7. This section presents parameters of the sensor in Fig 2 which can be fabricated to work on cast iron; it follows our work presented in [25]. The sensor consists of circular, air cored, concentrically wound coils acting as the exciter and detector coils and the holds on which the coils are wound were made of Polylactide (PLA) biodegradable polyester.

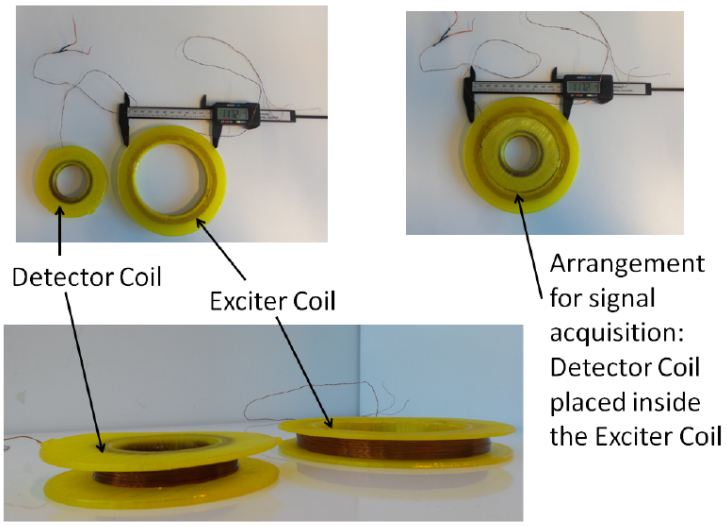

Figure 2: Fabricated PEC sensor, image adapted from [25].

The 2D Axisymmetric cross sectional view of the sensor when placed on a block like test piece is shown in Fig 3 as drawn in COMSOL Multiphysics®. Table 1 provides parameter values of the fabricated sensor referring to the unknowns marked in Fig 3; the values were deduced through simulation [25] to work on cast iron by being sensitive to thickness values of up to about 20 mm. Both exciter and detector coils were wound from insulated copper wires.

For grey cast iron, we excited the sensor with a voltage pulse train of 10 V amplitude, 100 ms period and 50% duty ratio. Detector coil signals were passed

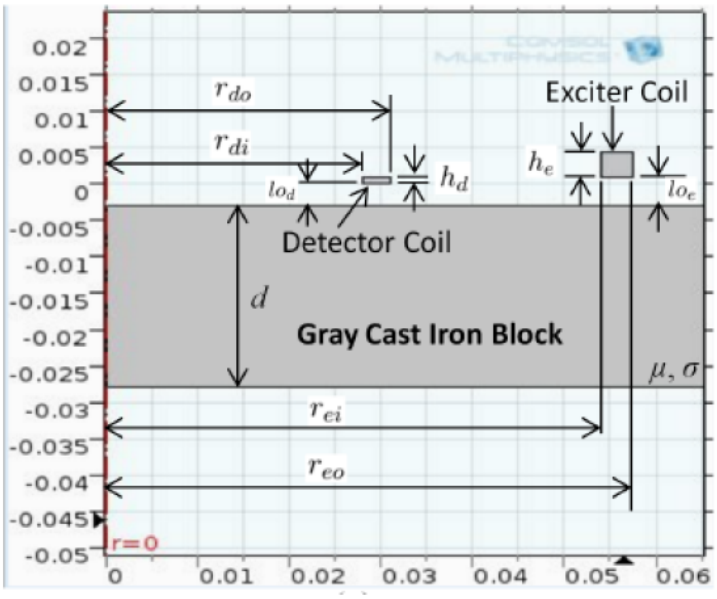

Figure 3: 2D Axisymmetric model of the PEC sensor placed on a cast iron block., image adapted from [25].

through an instrumentation amplifier of gain 1500. A single measurement was composed by averaging signals resulting from 10 consecutive pulses to reduce noise.

To demonstrate the signal behaviour, we collected data using the sensor on grey cast iron blocks having thickness 7 mm, 11 mm, 15 mm and 20 mm, with the sensor resting on the blocks with no added lift-off. The blocks were machined from an in situ aged pit cast iron pipe asset reported in [7]. Length and width of each block was 30 mm and 20 mm respectively; that size was determined beforehand through simulation to be large enough for signals to not be influenced by the edge effect.

The signals observed from the circular sensor along with the ones captured from the rectangular sensor coming with the HSK 300 commercial module are shown in Fig 4. Although signal amplifier saturation points and gains appear to be different for the two sensing set-ups, it is evident that signals from both sensors are parallel in their late phases, indicating that they produce similar

Table 1: Description of sensor parameters, adapted from [25].

Symbol	Description (mm)	Value
r_{di}	Inner radius of detector coil domain	25 mm
r_{do}	Outer radius of detector coil domain	28 mm
h_d	Height of detector coil domain	10 mm
lo_d	Vertical offset of the detector coil	2 mm
n_d	Number of detector coil turns	300
d_d	Diameter of the detector coil wire	0.315 mm
r_{ei}	Inner radius of exciter coil domain	50 mm
r_{eo}	Outer radius of exciter coil domain	57 mm
h_e	Height of exciter coil domain	10 mm
lo_e	Vertical offset of the exciter coil	2 mm
n_e	Number of exciter coil turns	600
d_e	Diameter of the exciter coil wire	0.315 mm

β_{max} values. Fig. 5 shows the function between β_{max} and thickness observed from the two sensors. Interested readers can attempt to fabricate and use the sensor presented in this section if working on cast irons, or else follow the design procedure presented in [25] and produce a similar circular sensor which may suit different materials or sensor size requirements.

4. Finite Element Analysis (FEA) validation for pipes

The FEA simulations discussed in this section were based on the PEC sensor employed, the HSK 300 commercial PEC signal capturing module [22] which was used for all experiments on in situ pipes along with the 50 mm single receiver hand held sensor shown in Fig. 6 (a). Apart from the sensor, the module consists of an application specific signal acquisition unit and a computer interface to save the signals.

For simplicity, the relationship for $\beta(t)$ was derived for conducting plates.

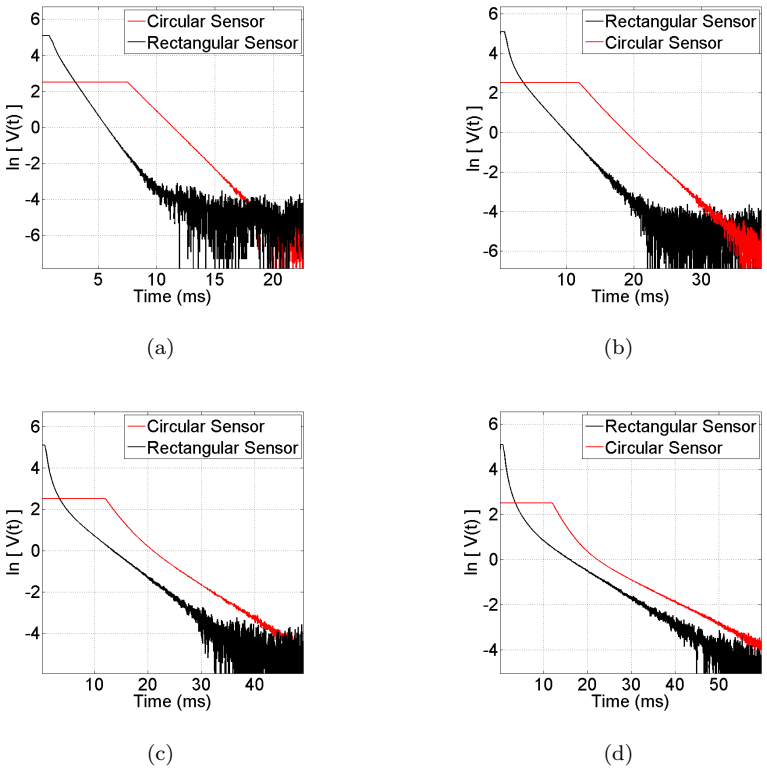

Figure 4: Signals produced by the circular and rectangular sensors on grey cast iron: (a) 7 mm thickness, (b) 11 mm thickness, (c) 15 mm thickness and (d) 20 mm thickness.

However, our intention was to use the decay rate as a signal feature for thickness quantification of cylindrical structures, i.e. large diameter in-situ pipes. It could be hypothesized that the plate approximation is reasonable given large dimater pipes investigated are of radius R greater than 250 mm while the sensor width used w is 50 mm in the direction perpendicular to the pipe axis, thus the surfaces would exhibit low curvature.

Verification of this hypothesis was performed through FEA on gray cast iron using material properties of a specimen extracted [7]. High precision magnetization curves and electrical conductivity were obtained using a Quantum Design Physical Property Measurement System (PPMS-9T). The FEA model was developed using COMSOL Multiphysics®; taking into account sensor properties

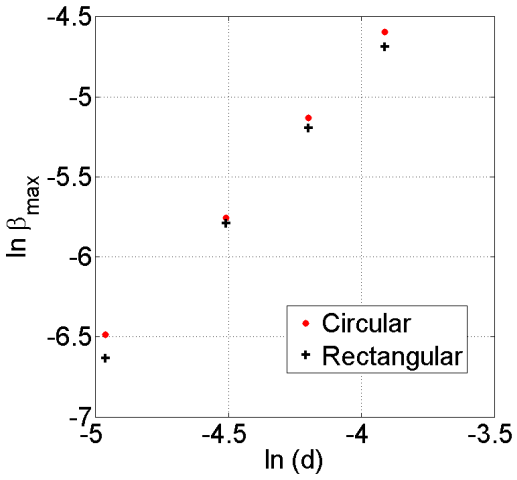

Figure 5: Function between β_{max} and thickness observed from the circular and rectangular sensors.

(physical dimensions, inherent properties and excitation signal characteristics) and test piece properties (physical dimensions, electrical and magnetic properties) as inputs and solves the magnetic vector potential equation to produce the sensor response. The 3D simulation model and FEA results against measurements obtained using the PEC sensor are shown in Fig. 7 and also reported as parts of [23] and [24].

In order to validate the invariance of the sensor signal to curvature of the cylindrical structure, the hypothesis tested is that for a given PEC sensor width w, there exists a range $w/R < k$ where $k \in \mathbb{R}^+$, such that the variation of β_{max} due to the curvature of the test piece remains insignificant. It was noted that k depends on electromagnetic properties of the material being tested, sensor architecture and excitation signal characteristics. For practical quantification, we defined the range of interest where the curvature dependent variation of β_{max} for any thickness of interest is less that 1% from the flat plate reference. From the analysis reported in Fig. 8, the pipe radii which satisfy $w/R < 0.25$ produce β_{max} variations less than 1% for our sensor. Given the minimum radius of the pipes scanned in this work was 250 mm the maximum w/R value encountered

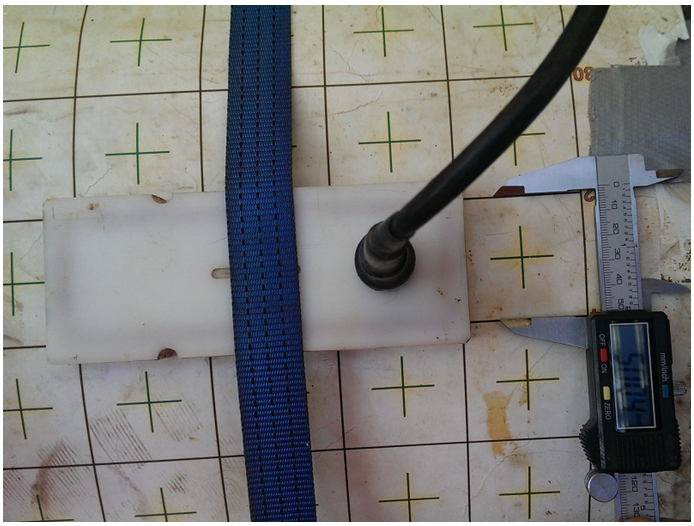

(a)

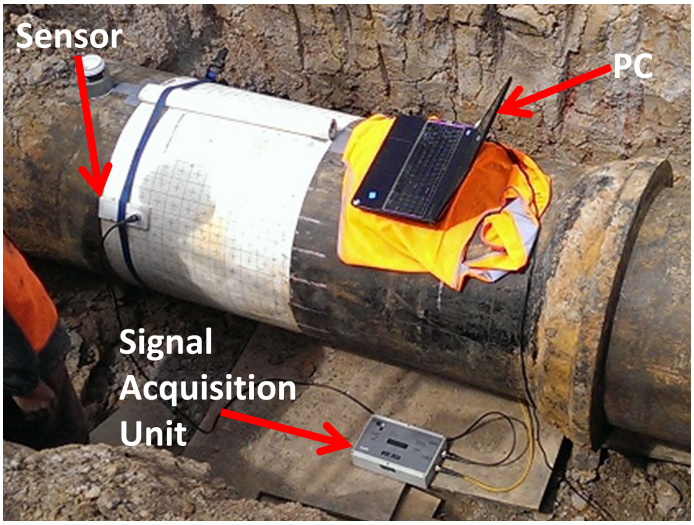

(b)

Figure 6: PEC signal capturing module: (a) PEC sensor, (b) The module being used in situ.

was 0.2 ($w = 50$ mm and $R = 250$ mm), thus the approximation of large diameter pipe surfaces as flat plates holds for practical purposes.

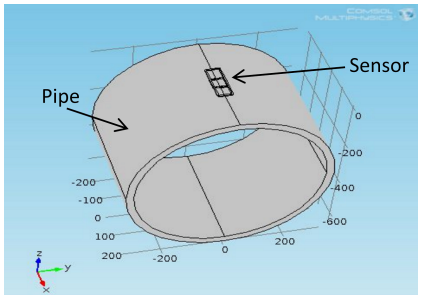

(a)

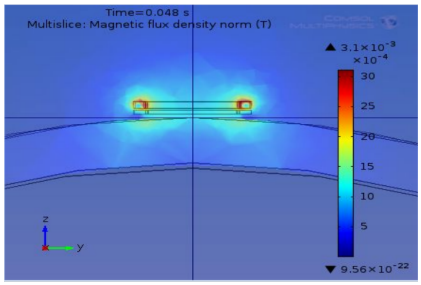

(b)

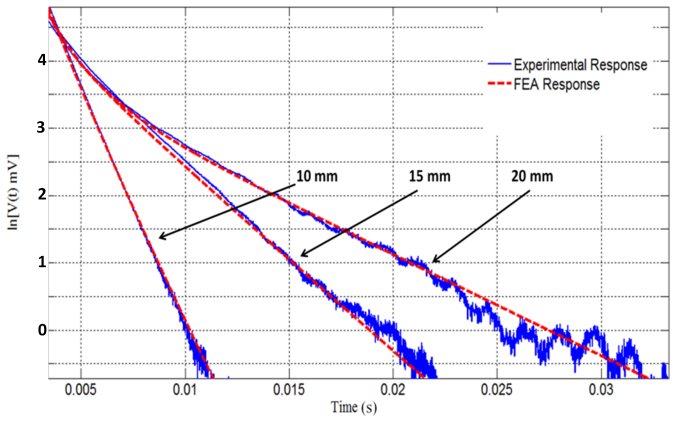

(c)

Figure 7: Numerical PEC sensor simulation model: (a) 3D model of the sensor and pipe, (b) Cross section showing induced fields, (c) Simulated sensor responses against unfiltered experimental signals for a range of thicknesses.

5. Experimental validation on a range of ferromagnetic materials

Experimental validation of the analytically derived linear relationship in Eq. 8 was done using signals acquired on ferromagnetic calibration blocks having known thicknesses. Length and width of calibration blocks were made three times the length and width of the sensor respectively to avoid edge effect; the required calibration block size for the particular sensor used was determined through FEA simulations [24]. We estimated c for the three critical pipe ma-

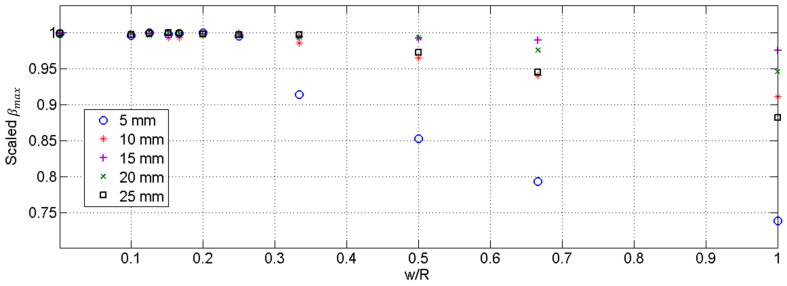

Figure 8: Effect of curvature on β_{max} for different thicknesses of gray cast iron.

terials gray cast iron, ductile cast iron and mild steel and validated the linear behavior with the intention of using the linear models for condition assessment of in situ critical pipes. Block thickness ranges were selected based on maximum available wall thickness of commercially used ferromagnetic water pipes corresponding to each material and are reported in Table 2.Three raw PEC measurements were taken on each block to capture system noise. The late phase gradient β_{max} was computed from the signals by fitting a straight line to the region $0 < \ln[V(t)] < 2$ as explained in Section 2.

Table 2: Ferromagnetic material calibration block thicknesses.

Material	Thicknesses (mm)
Mild Steel	3, ..., 12
Ductile Cast Iron	3, 5, 6, 8, ..., 18
Gray Cast Iron	3, 4, ..., 10, 12, ..., 22, 25, 30

5.1. Behavior of the Decay Rate

Fig. 9 shows the full set of PEC signals obtained for Mild Steel with the considered noise margin of $\ln[V(t)] = 0$ marked. Behaviors that are quantitatively different, but qualitatively identical to those of Fig. 9 were observed for ductile and gray cast irons [24]. The result in Fig. 10 demonstrates the linear relationship between $\ln \beta_{max}$ and $\ln d$ observed in calibration data for a range

of thicknesses of pipe materials. As mentioned, three readings were obtained on each block, thus, the inherent noise of β_{max} for each material can be visualized as the spread of $\ln \beta_{max}$ for a given thickness in the form of $\ln d$.

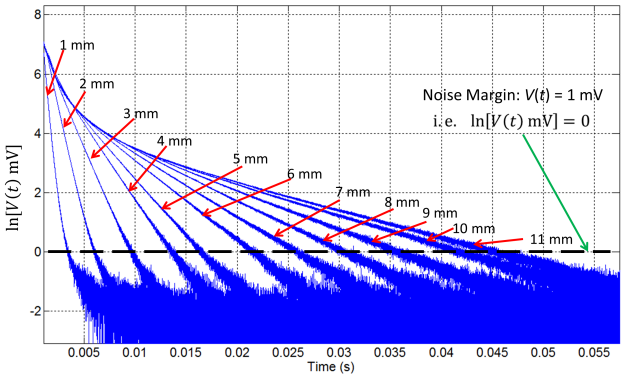

(a)

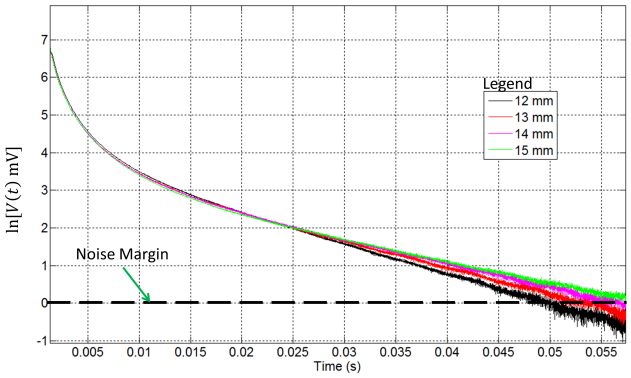

(b)

Figure 9: Decaying part of raw PEC signals for Mild Steel: (a) Low thicknesses, (b) High thicknesses.

5.2. Linear Behavior of the Thickness-Feature Function

Despite noise, the behavior of $\ln \beta_{max}$ is almost linear with $\ln d$ for all materials and the model parameter c given in Table 3 was obtained by averaging $\ln \beta_{max} - 2 \ln d$ values extracted from data. The Root Mean Square (RMS) error of each fit is also given in Table 3. Fitted lines are shown in the form

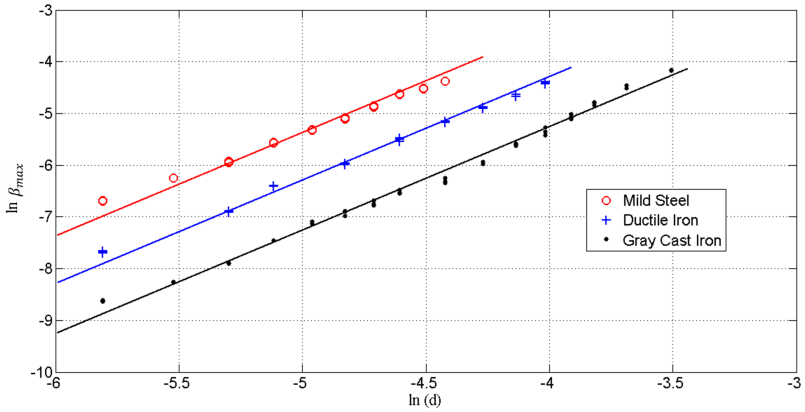

Figure 10: Linear relationship between $\ln \beta_{max}$ and $\ln d$ for different ferromagnetic materials.

of continuous lines in Fig. 10. The resulted c values specify parametric models which map β_{max} of the PEC induced detector coil voltage to the thickness of a considered material. Moreover, c values can be used to get an indication of electromagnetic properties of the material in the form of $\mu\sigma \approx \pi^2 \exp(c)$ in Table 3. Understandably, $\mu\sigma$ values are in ascending order for gray cast iron, ductile cast iron and mild steel since their electrical conductivities and magnetic permeabilities follow this order [26]. The linear models were also tested on in situ gray and ductile cast iron pipes and the results are reported in the following sections.

Table 3: Parameters of fitted straight lines for $\ln \beta_{max}$ vs $\ln d$ variation of different materials.

Material	c	RMS Error	$\mu\sigma$
Gray Cast Iron	2.7473	0.1109	153.973
Ductile Cast Iron	3.7143	0.09819	404.940
Mild Steel	4.6330	0.1324	1014.829

5.3. Experimentally Observable Nonlinearity in the Low and High Thicknesses

Theory suggests perfect linearity between $\ln d$ and $\ln \beta_{max}$. However, experiments demonstrate that the thickness range in which the linearity can be observed is finite. Experiments yield nonlinearities in the low and high thickness ends, Fig. 11 depicts the behavior of ductile cast iron while similar characteristics were observed on other ferromagnetic materials.

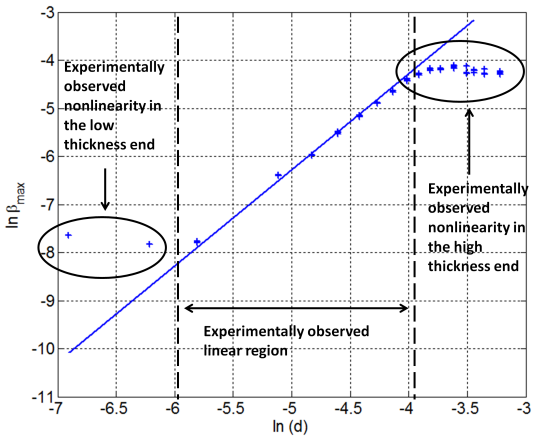

Figure 11: Experimentally observable nonlinearity in low and high thickness ends (ductile cast iron).

The nonlinearity is a result of the sensor size and excitation, which is optimally selected to discriminate the ranges of thicknesses anticipated for large diameter ferromagnetic pipes. In the high thickness end, the nonlinearity is caused by the limitation of the sensor's penetration capability for a fixed excitation strength. Nonlinearity in the low thickness end is due to signals entering the noise margin before they attain the constant gradient (i.e. linear) phase. The proposed linear model cannot capture the nonlinearities. However, since the intended application is pipe condition assessment, these nonlinearities did not prove to be greatly adverse as the existence of very low thicknesses (i.e. 1 to 3 mm) and very high thicknesses (values depend on the material being tested, 18 mm for Ductile Iron noted in Fig.11) of pipe walls are not present. For practical purposes, authors followed the process of fitting the linear model

in Eq. 8 to all data captured for a material and sequentially removing lowest and highest thickness points until a fit with an RMS error of less than 0.15 was obtained

6. Non Destructive Evaluation of in situ pipes

6.1. PEC based Thickness Interpretation

Data from in-situ pipes were obtained by scanning full circumference of several in situ cast iron and ductile iron pipe segments in collaboration with a local water utility [7]. Steel pipes were not available to be scanned at the time of experiments. Axial length of scanned segments was 1 m. In situ scanning being done is shown in Fig. 6 (b). Scanning was done with the aid of a grid of squares wrapped around the pipe, side length of a square was 50 mm. Scans were obtained by spanning the full circumference of 1 m long pipe segments by centralizing the detector coil on each square. The decay rates of these signals were also calculated and pipe wall thickness maps were produced using the transformation $d = \exp\left(\frac{\ln \beta_{max} - c}{2}\right)$.

For validation of the interpretation of thickness, pipe segments were grit blasted both internally and externally to remove rust and deterioration, laser scanned to obtain point clouds and then subsequently up-sampled and ray traced to calculate precise wall thickness profiles at a resolution of 0.8 mm [27]. High resolution profiles were averaged to match the resolution of the PEC sensor to compare the accuracy of the thickness estimates.

Fig. 12 and 13 show the interpreted pipe wall thickness maps of two 1 m long gray cast iron pipe segments along with their Ground Truth (GT). The level of agreement between the interpretations and GT is presented in Fig. 14, an ideal curve taking the form of $y = x$ is noted and the interpretation against GT appears as scatter. Statistical parameters of errors were therefore quantified and are presented in Table 4. A mean percentage accuracy of over 90% was observed for gray cast iron. Similarly, a 1 m long ductile cast iron pipe segment was tested and results are presented in Fig. 15 and 16 while the sta-

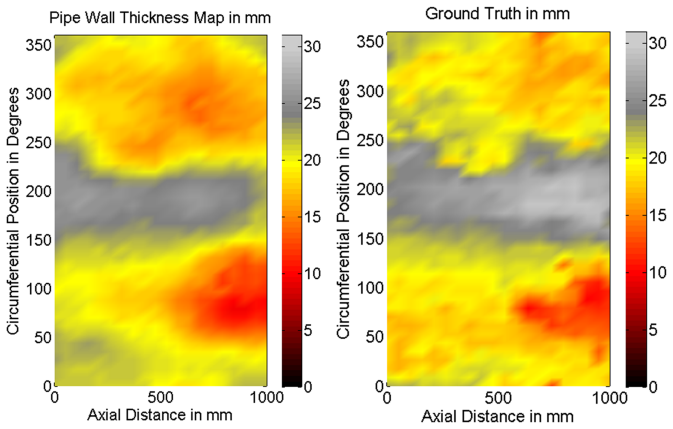

Figure 12: Interpreted thickness map and GT for the first Gray Cast Iron pipe segment.

tistical error analysis results are given in Table 5. Achieved mean percentage accuracy was over 94%. Since all interpreted thicknesses showed the property $|\text{Interpretation} - \text{GT}| < \text{GT}$, the mean percentage accuracies in Tables 4 and 5 were obtained by computing $\left(1 - \dfrac{|\text{Interpretation} - \text{GT}|}{\text{GT}}\right) \times 100\%$ for each individual interpretation and then calculating their mean.

Although the relationship between $\ln \beta_{max}$ and $\ln d$ was modelled through experiments in this work, simplification of that approach is possible since the

Table 4: Statistics of absolute error between interpreted pipe wall thickness maps and ground truth for Gray Cast Iron pipe segments.

Statistical Parameter	Value
RMS Error	2.42 mm
Mean Absolute Error	2.00 mm
Standard Deviation of Absolute Error	1.37 mm
Maximum Absolute Error	7.06 mm
Mean Percentage Accuracy	90.3%

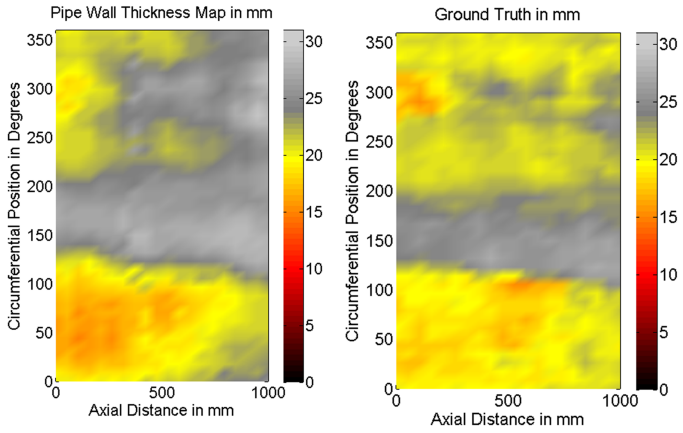

Figure 13: Interpreted thickness map and GT for the second Gray Cast Iron pipe segment.

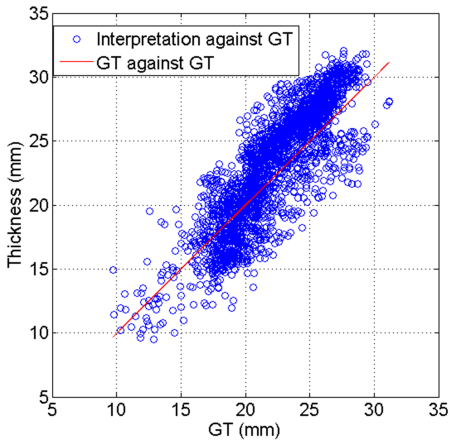

Figure 14: Variation of interpretations along with GT for the Gray Cast Iron pipe segments.

decay rate can be simulated using computational methods such as FEA, as part of our previous work [23] and in Section 2. Such an approach will be immensely helpful to commercial PEC service providers by reducing the requirement of fabricating calibration blocks.

If the models are learned from a certain set of calibration blocks, the material

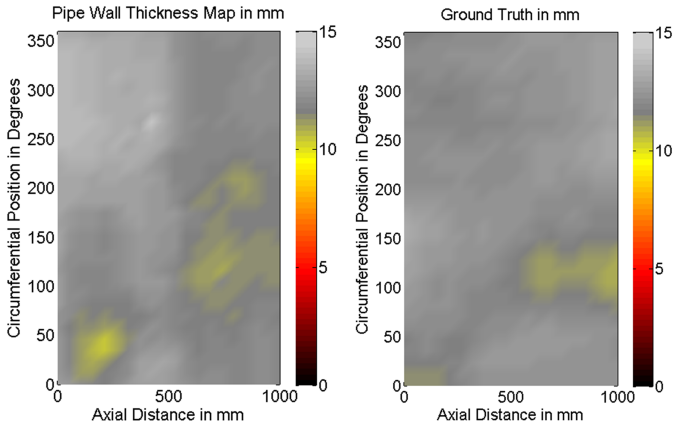

Figure 15: Interpreted thickness map and GT for the Ductile Cast Iron pipe segment.

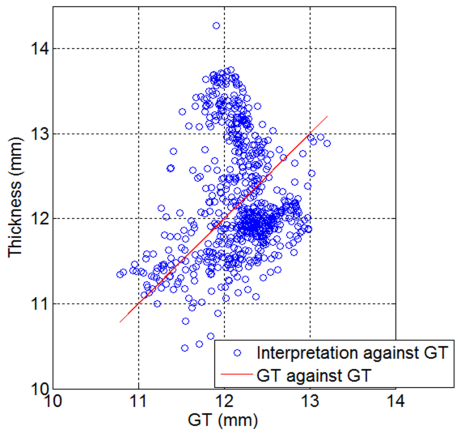

Figure 16: Variation of interpretations along with GT for the Ductile Cast Iron pipe segment.

properties embedded within c will be unique to pipes of similar properties. In reality, material properties may change even in pipes made of the same material (gray cast iron for instance) depending on manufacturing methods and previous electromagnetic interactions they have been subjected to. In such instances, a model learned from one set of calibration blocks may not be sufficiently universal

Table 5: Statistics of absolute error between interpreted pipe wall thickness map and ground truth for the Ductile Cast Iron pipe segment.

Statistical Parameter	Value
RMS Error	0.755 mm
Mean Absolute Error	0.616 mm
Standard Deviation of Absolute Error	0.438 mm
Maximum Absolute Error	2.359 mm
Mean Percentage Accuracy	94.93%

for thickness quantification of all pipes of the same material. This challenge can be overcome by calibrating the c value using $c = (\ln \beta_{max} - 2 \ln d)$ using one or a few known thicknesses on a pipe. Performing destructive testing to obtain calibrations thicknesses on in situ pipes by cutting out samples large enough for the PEC sensor is not feasible. However, using techniques such as ultrasounds is a feasible option after cleaning the pipe surface on suitable locations to expose healthy metal and achieve sufficient connectivity as per Fig. 17. Alternatively, extracting tiny samples and using SQUID or PPMS devices to precisely measure electrical and magnetic properties and numerically simulating the decay rates as per Section 2 for calibration is viable.

6.2. Ultrasound aided PEC based Thickness Interpretation

The possibility of using ultrasound measurements to calculate c and estimate the full thickness map of a 1 m long gray cast iron pipe segment was examined in this work. Since the relationship $\ln \beta_{max} = 2 \ln d + c$ is established, $\ln \beta_{max}$ values corresponding to a pipe segment were plotted as per Fig. 19 and a region containing high $\ln \beta_{max}$ values was identified. The size of the identified high feature value region was set to 10 cm$\times$10 cm. 16 ultrasound measurements were performed in the region using a calibrated direct contact ultrasound probe of diameter 2.5 cm. The square was cleaned before performing ultrasound measurements to achieve good connectivity. Each ultrasound based thicknesses

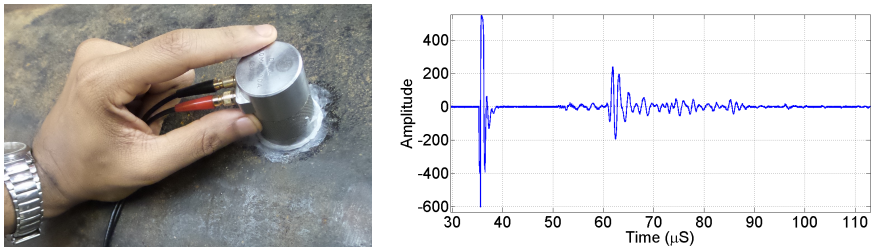

(a) (b)

Figure 17: Measuring pipe wall thickness using ultrasounds after cleaning the surface: (a) Ultrasound probe on pipe, (b) An ultrasound waveform.

was estimated using the kernel fitting method proposed in [28], and an average thickness was calculated for the square. Similarly, an average $\ln \beta_{max}$ value was also calculated for the square using the PEC signals. The average thickness and $\ln \beta_{max}$ values were 25.1301 mm and -4.688 respectively, using $c = \ln \beta_{max} - 2 \ln d$ resulted in a calibration value for c of 2.6794. This value was subsequently used in the transformation $d = \exp\left(\frac{\ln \beta_{max} - c}{2}\right)$ to estimate the full thickness map. Results are shown in Fig. 20 and Fig. 21. Table 6 shows the error statistics, the percentage accuracy was over 94%, which was slightly better than 92% for the same pipe section when thickness was estimated using $c = 2.7473$, the c value resulting from calibration blocks. Therefore, the approach can be considered a practically effective method to reduce the errors caused by material property discrepancies. Ultrasound probes were calibrated as shown in Fig. 18 with the aid of small coupons having known thickness extracted from a pipe.

(a) (b)

Figure 18: Calibrating the Ultrasound probe: (a) Coupons having known thickness, (b) Calibration being performed.

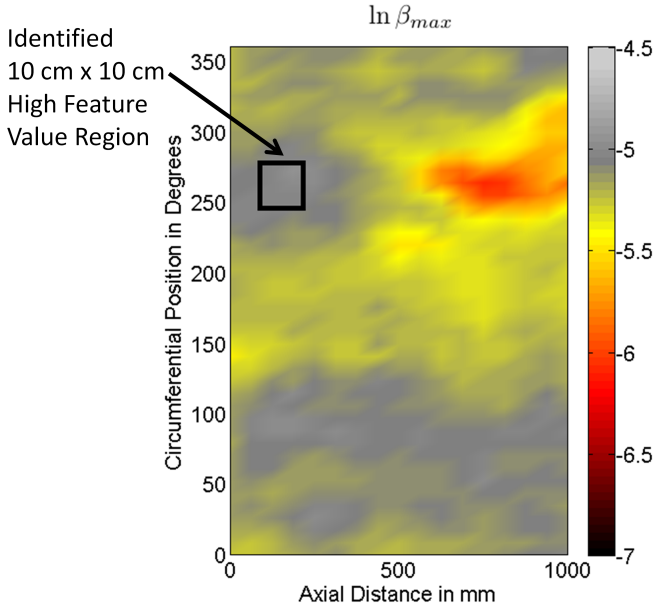

Figure 19: Plot of $\ln \beta_{max}$ values for data obtained on a gray cast iron pipe segment

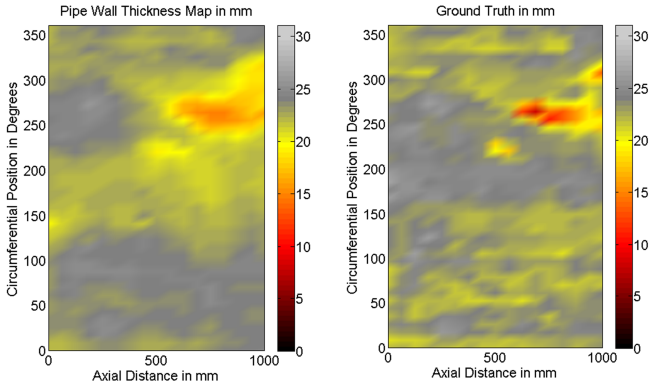

Figure 20: Interpreted thickness map (by estimating c using ultrasounds) and GT for a Gray Cast Iron pipe segment.

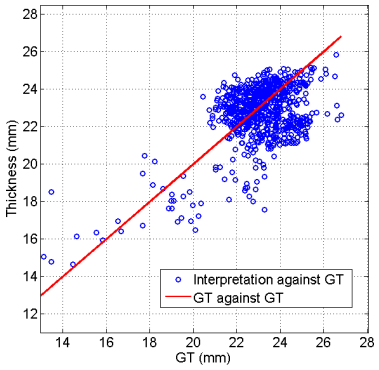

Figure 21: Variation of interpretations (by estimating c using ultrasounds) along with GT for a Gray Cast Iron pipe segment.

6.3. Sensitivity analysis of β_{max} with respect to lift-off

Arising of the requirement to perform condition assessment of metals protected by an insulated coating is quite common in PEC applications. Lift-off insensitivity of a signal feature used for thickness quantification is desired in such applications. In relation to critical pipes, there are instances where the internal pipe wall is coated by a cement lining and this requires PEC sensors to estimate wall thickness while cement linings behave as lift-off.

To examine the performance of β_{max} in the presence of lift-off, we inves-

Table 6: Statistics of absolute error between interpreted pipe wall thickness map (by estimating c using ultrasounds) and ground truth for a Gray Cast Iron pipe segment.

Statistical Parameter	Value
RMS Error	1.62 mm
Mean Absolute Error	1.25 mm
Standard Deviation of Absolute Error	1.02 mm
Maximum Absolute Error	7.41 mm
Mean Percentage Accuracy	94.39%

tigated the variation of β_{max} with lift-off on gray cast iron calibration blocks having different thicknesses. Lift-off was created using perspex plates having known thicknesses and Fig. 22 shows the observed results.

According to Fig. 22, it can be observed that β_{max} possesses a considerable insensitivity to lift-off, which is an advantage. As the intended application is pipe condition assessment, the main interest is on the low thickness ranges where β_{max} is less sensitive to lift-off.

7. Conclusions

The main objective of this paper was to propose a method for estimating thickness of ferromagnetic materials, in particular that of large diameter critical ferrous pipe infrastructure of water utilities. A PEC sensor detector coil voltage decay rate based ferromagnetic material thickness quantification method was presented. The relationship between the decay rate gradient and the thickness was analytically derived and the properties of the relationship were experimentally verified. The applicability of the decay rate on estimation of cylindrical structures was validated through Finite Element Analysis and subsequently experimentally confirmed. Parameters of the relationship were quantified for three ferromagnetic pipe materials: gray cast iron, ductile cast iron and mild steel, using experimental data obtained from a commercial PEC signal capturing mod-

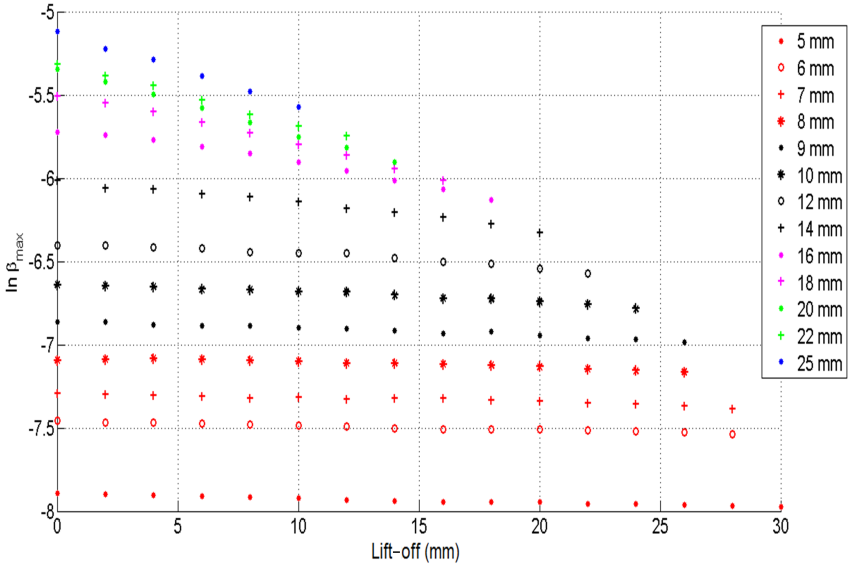

Figure 22: Experimentally observed considerable lift-off insensitivity of β_{max} for gray cast iron.

ule. The modeled relationships were then used for wall thickness quantification of in situ gray and ductile cast iron pipes. Comparison of the interpreted thickness and actual pipe thickness obtained via laser scanning after graphitisation removal yielded a percentage accuracy of over 90%, confirming the usability of the proposed method for NDE of in situ ferromagnetic pipes.

Learning relationships using standard calibration blocks and applying them on complex environments such as in situ pipes may affect the accuracy of thickness estimates due to the variation of electrical and magnetic properties between materials. This effect can be nullified by obtaining readings on one or few known thicknesses of the exact material being tested and calibrating the model. Alternatively, calibrating PEC feature values using ultrasound measurements performed on cleaned and smoothened surfaces, or extracting precise electromagnetic properties by using magnetic measurement systems and simulating PEC signals is possible.

Since detector coil based PEC sensors are limited in resolution, an estimated thickness value becomes a representation of average wall thickness within a cell governed by the sensor coil sizes. The proposed thickness quantification method has the potential to be used in conjunction with high resolution methods by making PEC sensors sufficiently small or perturbing large sensors within close proximity. It may also be feasible to combine this method with lift-off quantification techniques to obtain detailed 3D pipe profiles.

Acknowledgment

This publication is an outcome from the Critical Pipes Project funded by Sydney Water Corporation, Water Research Foundation of the USA, Melbourne Water, Water Corporation (WA), UK Water Industry Research Ltd, South Australia Water Corporation, South East Water, Hunter Water Corporation, City West Water, Monash University, University of Technology Sydney and University of Newcastle. The research partners are Monash University (lead), University of Technology Sydney and University of Newcastle. The authors would also like to acknowledge the contribution from the Rock Solid Group© in providing the PEC signal capturing module and access to data used in this research.

References

[1] J. García-Martín, J. Gómez-Gil, E. Vázquez-Sánchez, Non-destructive techniques based on eddy current testing, Sensors 11 (3) (2011) 2525–2565. doi:10.3390/s110302525.

[2] X. Chen, D. Hou, L. Zhao, P. Huang, G. Zhang, Study on defect classification in multi-layer structures based on fisher linear discriminate analysis by using pulsed eddy current technique, NDT & E International 67 (2014) 46–54. doi:10.1016/j.ndteint.2014.07.003.

[3] Z. Liu, Y. Kleiner, State of the art review of inspection technologies for condition assessment of water pipes, Measurement 46 (1) (2013) 1–15. doi:10.1016/j.measurement.2012.05.032.

[4] A. Sophian, G. Y. Tian, D. Taylor, J. Rudlin, Flaw detection and quantification for ferromagnetic steels using pulsed eddy current techniques and magnetization, Transactions on Engineering Sciences 44 (2003) 381–390. doi:10.2495/LAMDAMAP030331.

[5] W. Cheng, Pulsed eddy current testing of carbon steel pipes wall-thinning through insulation and cladding, Journal of Nondestructive Evaluation 31 (3) (2012) 215–224. doi:10.1007/s10921-012-0137-9.

[6] W. Guo, L. Soibelman, J. Garrett Jr, Automated defect detection for sewer pipeline inspection and condition assessment, Automation in Construction 18 (5) (2009) 587–596. doi:10.1016/j.autcon.2008.12.003.

[7] J. V. Miro, J. Rajalingam, T. Vidal-Calleja, F. de Bruijn, R. Wood, D. Vitanage, N. Ulapane, B. Wijerathna, D. Su, A live test-bed for the advancement of condition assessment and failure prediction research on critical pipes, Water Asset Management International, ISSN Print: 1814-5434, ISSN Online: 1814-5442 10 (2) (2014) 03–08.

[8] Z. Xu, X. Wu, J. Li, Y. Kang, Assessment of wall thinning in insulated ferromagnetic pipes using the time-to-peak of differential pulsed eddy-current testing signals, NDT & E International 51 (2012) 24–29. doi:10.1016/j.ndteint.2012.07.004.

[9] G. Y. Tian, Y. Li, C. Mandache, Study of lift-off invariance for pulsed eddy-current signals, Magnetics, IEEE Transactions on 45 (1) (2009) 184–191. doi:10.1109/TMAG.2008.2006246.

[10] C. Angani, D. Park, G. Kim, C. Kim, Y. Cheong, Differential pulsed eddy current sensor for the detection of wall thinning in an insulated stainless steel pipe, Journal of Applied Physics 107 (9) (2010) 09E720. doi:10.1063/1.3337725.

[11] Y. He, M. Pan, F. Luo, G. Tian, Pulsed eddy current imaging and frequency spectrum analysis for hidden defect nondestructive testing and evaluation,

NDT & E International 44 (4) (2011) 344–352. doi:10.1016/j.ndteint.2011.01.009.

[12] A. Sophian, G. Y. Tian, D. Taylor, J. Rudlin, A feature extraction technique based on principal component analysis for pulsed eddy current ndt, NDT & E International 36 (1) (2003) 37–41. doi:10.1016/S0963-8695(02)00069-5.

[13] G. Y. Tian, A. Sophian, D. Taylor, J. Rudlin, Multiple sensors on pulsed eddy-current detection for 3-d subsurface crack assessment, IEEE Sensors Journal 5 (1) (2005) 90–96. doi:10.1109/JSEN.2004.839129.

[14] D. Park, C. Angani, G. Kim, C. Kim, Y. Cheong, Evaluation of pulsed eddy current response and detection of the thickness variation in the stainless steel, Magnetics, IEEE Transactions on 45 (10) (2009) 3893–3896. doi:10.1109/TMAG.2009.2024219.

[15] D. Chen, Q. Ji, H. Zhang, L. Zhao, Application of pulsed eddy current in plate thickness evaluation, in: Proceedings of the 4th IEEE Conference on Industrial Electronics and Applications, IEEE ICIEA, IEEE, 2009, pp. 3286–3288. doi:10.1109/ICIEA.2009.5138810.

[16] D. Vasic, V. Bilas, D. Ambrus, Pulsed eddy-current nondestructive testing of ferromagnetic tubes, Instrumentation and Measurement, IEEE Transactions on 53 (4) (2004) 1289–1294. doi:10.1109/TIM.2004.830594.

[17] C. Huang, X. Wu, Z. Xu, Y. Kang, Ferromagnetic material pulsed eddy current testing signal modeling by equivalent multiple-coil-coupling approach, NDT & E International 44 (2) (2011) 163–168. doi:10.1016/j.ndteint.2010.11.001.

[18] M. Fan, P. Huang, B. Ye, D. Hou, G. Zhang, Z. Zhou, Analytical modeling for transient probe response in pulsed eddy current testing, NDT & E International 42 (5) (2009) 376–383. doi:10.1016/j.ndteint.2009.01.005.

[19] Y. Li, G. Y. Tian, A. Simm, Fast analytical modelling for pulsed eddy current evaluation, NDT & E International 41 (6) (2008) 477–483. doi:10.1016/j.ndteint.2008.02.001.

[20] C. Huang, X. Wu, An improved ferromagnetic material pulsed eddy current testing signal processing method based on numerical cumulative integration, NDT & E International 69 (2015) 35–39. doi:10.1016/j.ndteint.2014.09.006.

[21] X. Chen, Y. Lei, Excitation current waveform for eddy current testing on the thickness of ferromagnetic plates, NDT & E International 66 (2014) 28–33. doi:10.1016/j.ndteint.2014.04.006.

[22] J. Rudd, M. Roubal, Broadband electro-magnetic technique for advanced condition assessment and pipe failure prediction of water infrastructure, in: Ozwater Conference, 2014. http://www.awa.asn.au/htmlemails/Ozwater14/pdf/natozw14Final00366.pdf, last access date: 11/01/2015.

[23] N. Ulapane, A. Alempijevic, T. Vidal-Calleja, J. V. Miro, J. Rudd, M. Roubal, Gaussian process for interpreting pulsed eddy current signals for ferromagnetic pipe profiling, in: Industrial Electronics and Applications (ICIEA), 2014 IEEE 9th Conference on, IEEE, 2014, pp. 1762–1767. doi:10.1109/ICIEA.2014.6931453.

[24] A. M. N. N. B. Ulapane, Nondestructive evaluation of ferromagnetic critical water pipes using pulsed eddy current testing, Ph.D. thesis (2016).

[25] N. Ulapane, L. Nguyen, J. V. Miro, G. Dissanayake, Designing a pulsed eddy current sensing setup for cast iron thickness assessment, in: Industrial Electronics and Applications (ICIEA), 2017 IEEE International Conference on, IEEE, 2017, Accepted.

[26] J. R. Davis, ASM specialty handbook: cast irons, ASM International 124 (1996) 433–435.

[27] B. Skinner, T. Vidal-Calleja, J. V. Miro, F. De Bruijn, R. Falque, 3D point cloud upsampling for accurate reconstruction of dense 2.5D thickness maps, in: Proceedings of the Australasian Conference on Robotics and Automation 2014 (ACRA 2014), Australian Robotics and Automation Association Inc., Melbourne, Australia, 2014, pp. 1–7.

[28] T. Vidal-Calleja, D. Su, F. De Bruijn, J. V. Miro, Learning spatial correlations for bayesian fusion in pipe thickness mapping, in: Robotics and Automation (ICRA), 2014 IEEE International Conference on, IEEE, 2014, pp. 683–690. doi:10.1109/ICRA.2014.6906928.